Supplementary Information

Microfluidic high-throughput selection of microalgal strains with superior photosynthetic productivity using competitive phototaxis

Jaoon Young Hwan Kim[1,†], Ho Seok Kwak[1,†], Young Joon Sung[1], Hong Il Choi[1], Min Eui Hong[1], Hyun Seok Lim[1], Jae-Hyeok Lee[2], Sang Yup Lee[3], and Sang Jun Sim[1,4,*]

[1]Department of Chemical and Biological Engineering, Korea University, Seoul, 136-713, Republic of Korea

[2]Department of Botany, University of British Columbia, Vancouver, V6T1Z4, Canada

[3]Department of Chemical and Biomolecular Engineering (BK21 Plus Program), BioProcess Engineering Research Center, Bioinformatics Research Center, Center for Systems and Synthetic Biotechnology, Institute for the BioCentury, Korea Advanced Institute of Science and Technology, Daejeon 305-701, Republic of Korea

[4]Green School, Korea University, Seoul, 136-713, Republic of Korea

*Corresponding author: simsj@korea.ac.kr

[†]These authors contributed equally to this work.

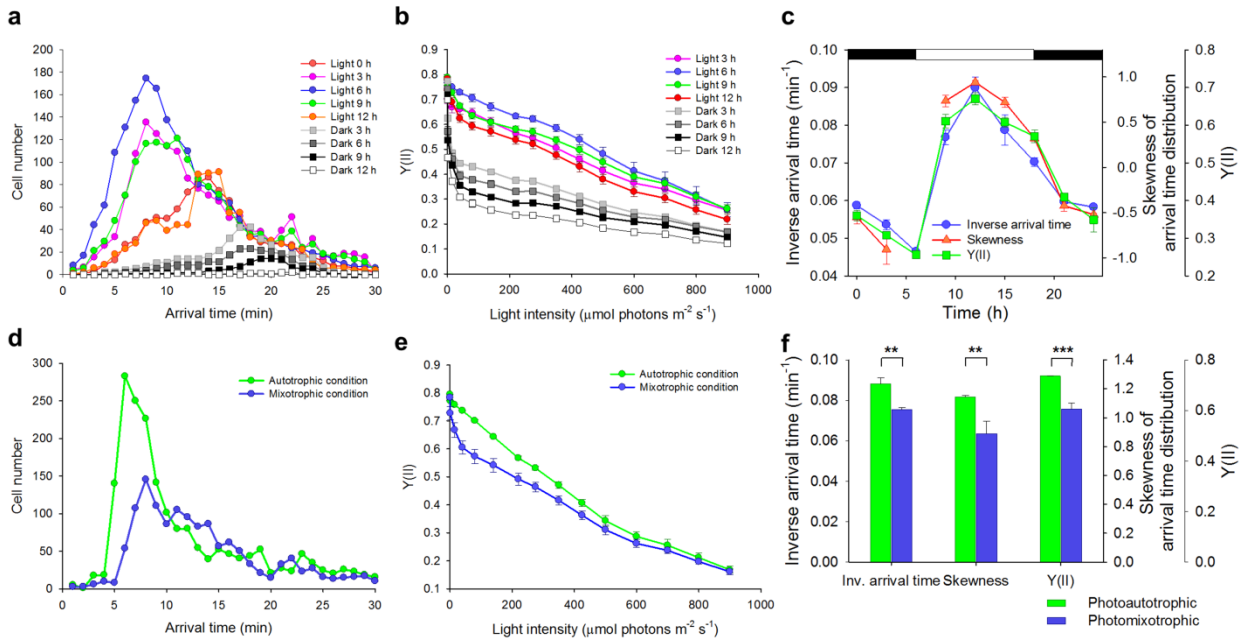

Supplementary Figure S1. Effect of circadian rhythm and trophic conditions on phototactic response and photosynthetic activity. (**a**) Distribution of the number of phototactic cells according to arrival time under LD cycle (12 h–12 h). Cells grown photomixotrophically in low light (50 µmol photons m^{-2} s^{-1}) were harvested every 3 h. The phototactic response was measured on 6,600 cells per analysis using microfluidic device. (**b**) PSII operating efficiency (Y(II)) measured under LD cycle (x-axis: stepwise-increases in actinic light from 1 to 900 µmol photons m^{-2} s^{-1}). (**c**) Skewness of arrival time distribution, inverse average arrival time of phototactic cells (wild type, CC125) and PSII operating efficiency (Y(II)) plotted against culture time under LD cycle (12 h light (white bar)–12 h dark (black bar)). Skewness of arrival time distribution at the end of dark phase (6 h) was not determined due to the near absence of a response. (**d**) Distribution of phototactic cell number according to arrival time under photoautotrophic (green) and photomixotrophic (blue) conditions. The phototactic response was measured on 6,600 cells per analysis. (**e**) PSII operating efficiency (Y(II)) measured under photoautotrophic (green) and photomixotrophic (blue) conditions (x-axis: stepwise-increases in actinic light from 1 to 900 µmol photons m^{-2} s^{-1}). (**f**) Skewness of arrival time distribution, inverse average arrival time of phototactic cells (wild type) and Y(II) under photoautotrophic conditions (green bars) compared to those under photomixotrophic conditions (blue bars). ** $P<0.01$; *** $P<0.001$, two-tailed Student's t-test. Cells were grown under continuous low light condition (50 µmol photons m^{-2} s^{-1}) (**d–f**). All data and error bars are the mean ± SD of three biological replicates.

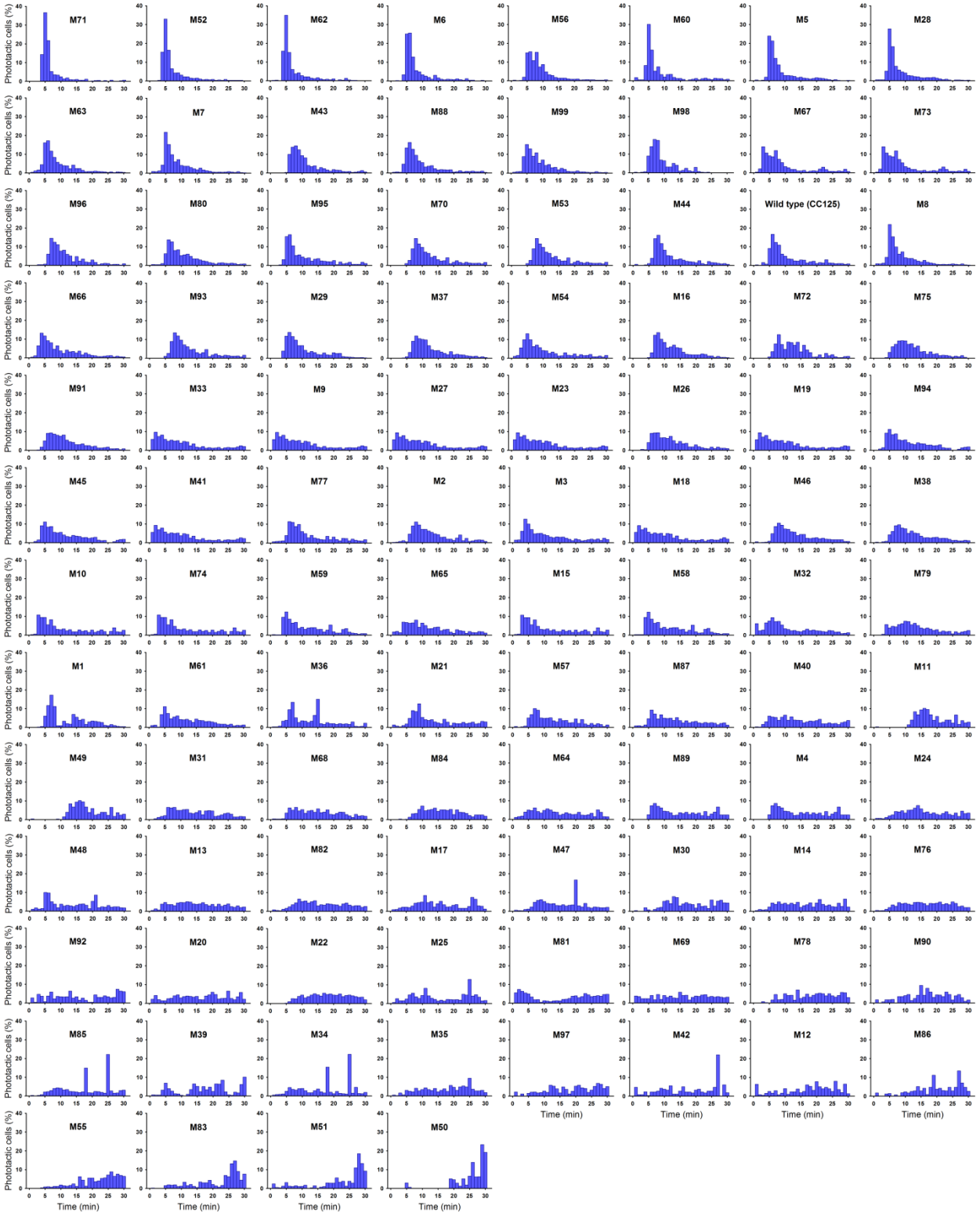

Supplementary Figure S2. Histograms showing the phototactic responses of 100 strains with different photosynthetic activities. The negative phototactic responses of 100 strains,

including the wild-type strain and 99 randomly selected mutants with a wide range of PSII operating efficiency (Y(II)), were analyzed, and histograms of phototactic cells (% of total phototactic cells) as a function of their arrival time are shown. Cells were grown photomixotrophically under continuous low light condition (50 μmol photons m^{-2} s^{-1}). The phototactic response was measured on 6,600 cells per analysis. All data are the mean of three biological replicates.

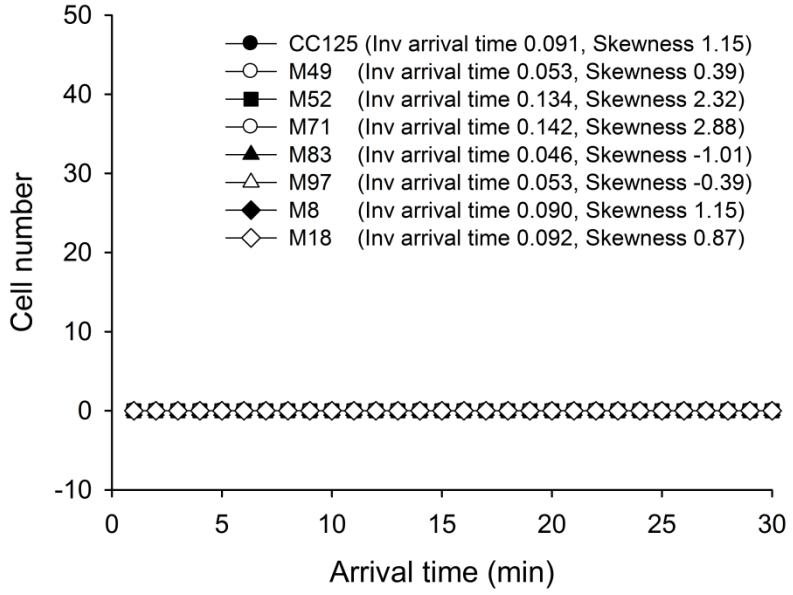

Supplementary Figure S3. Responses of various strains in microfluidic device without exposure to light stimulus. The responses of the wild-type strain and mutants with different phototactic responses were monitored without a light stimulus. Cells were grown photomixotrophically under low light condition (50 μmol photons m^{-2} s^{-1}). The response was measured on 6,600 cells per analysis. All data and error bars are mean ± SD of three biological replicates.

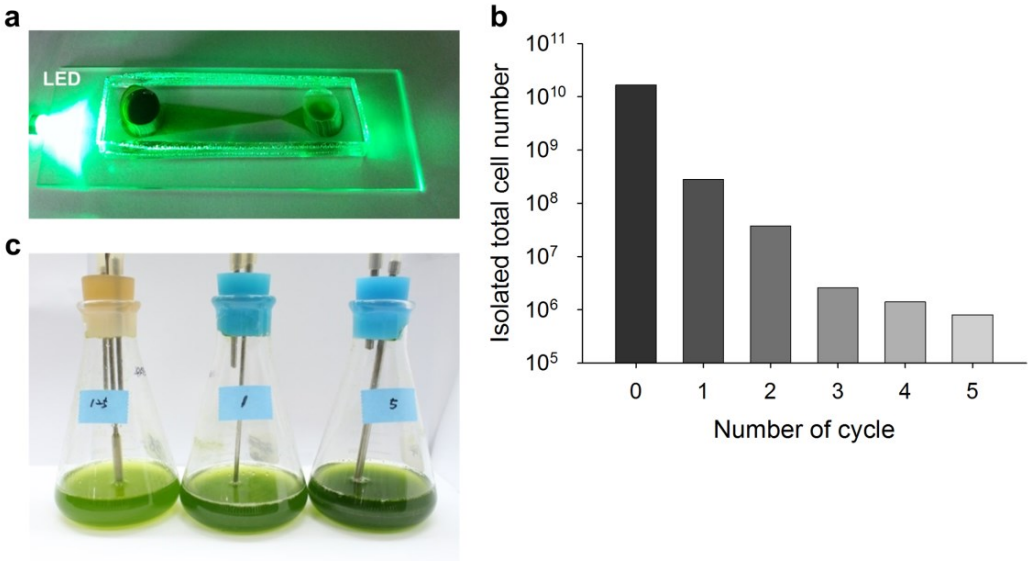

Supplementary Figure S4. Phototaxis-assisted screening. (**a**) Picture showing a microfluidic device with a green LED used for phototaxis-assisted screening. After dark-adaptation for 30 min, mutant mixture was loaded into the left chamber (dark green) and exposed to green LED light (70 µmol photons m^{-2} s^{-1}) for 10 min to isolate strains showing fast phototactic responses at the right chamber (light green). (**b**) Total number of cells isolated from mutant mixture after each cycle of screening. (**c**) Picture showing flask cultures of the wild-type strain and mutant mixtures obtained after 1 and 5 cycles of screening. The wild-type strain and mutant mixtures with the same initial cell densities (~1×10^4 cells/ml) were grown photoautotrophically under continuous low light condition (50 µmol photons m^{-2} s^{-1}).

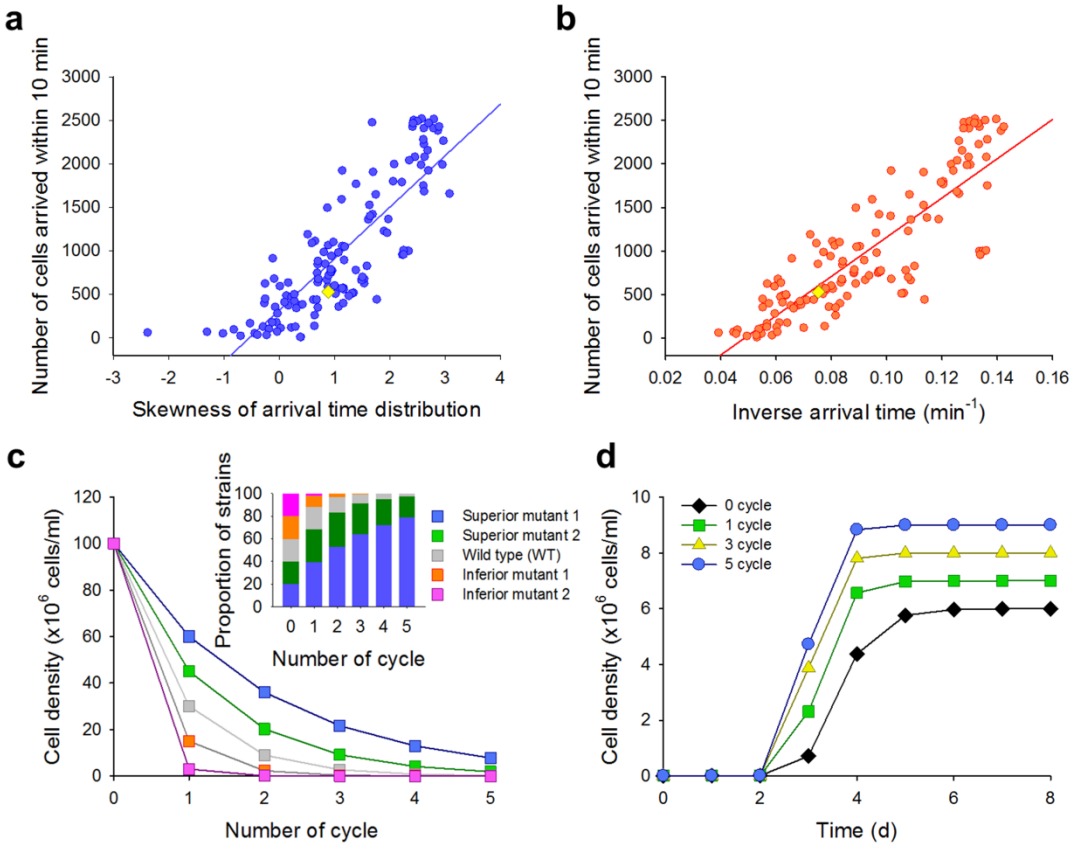

Supplementary Figure S5. A fast phototactic response provides a competitive advantage by increasing population and fitness. (**a**) Correlation between phototactic cell number of 136 strains arrived within 10 min and skewness of arrival time distribution (R^2 = 0.70). (**b**) Correlation between phototactic cell number of 136 strains arrived within 10 min and inverse average arrival time (R^2 = 0.73). The phototactic response was measured on 6,600 cells per analysis, and all data are the mean of three biological replicates. 136 strains include the wild-type strain (yellow diamond), 99 randomly selected mutant without phototaxis-assisted screening, and 36 strains isolated after five cycles of phototaxis-assisted screening (**a**,**b**). Cells were grown photomixotrophically under continuous low light condition (50 μmol photons m^{-2} s^{-1}). (**c**) Simplified model showing the changes in the cell densities of five strains with different phototactic responses in the phototaxis-assisted screening ($C_n = C_0(R_a \times R_p)^n$, where C_n is the cell density of each strain after n cycles of phototaxis-assisted screening; C_0 is the initial cell density of each strain before phototaxis-assisted screening (set to 1×10^8); R_a is the ratio of cell number arrived within 10 min to total cell number in the wild type (set to 0.3); R_p is the ratio between cell number arrived within 10 min in each mutant and the wild type (set to 2, 1, 0.5 and 0.1 for 4 mutants). The inset shows the population dynamics of each strain in the mixture of these strains according to number of screening cycle. The proportion of each mutant in the population was obtained from (**c**). Because the cell number arrived within 10 min depends on the rate of phototaxis (**a**,**b**), the population of strains showing fast responses increases as the number of screening cycle increases (**c** inset). (**d**) Simplified model showing growth curves for mixtures of

five strains after different number of screening cycle. The cell density of each mutant mixture after n cycles of screening was calculated using a modified Gompertz function[40], $C_n = C_0 \exp[A \cdot \exp\{-\exp(\mu_{max} \cdot e \cdot (\lambda - t)/A + 1)\}]$. The model assumes that the μ_{max} of strain mixture is average μ_{max} of strains (set to 2, 1.5, 1, 0.5 and 0.1), weighted by the proportion of each strain in the population after each cycle of phototaxis-assisted screening (**c**). A is the ratio of the final cell density of strain to the initial cell density ($\ln(C_f/C_0)$) after each cycle, which has the same meaning as the fitness of strain (set to 6.4, 6.55, 6.68 and 6.8 for 0, 1, 3 and 5 cycle based on the relatively high fitness of strains exhibiting fast phototactic responses).

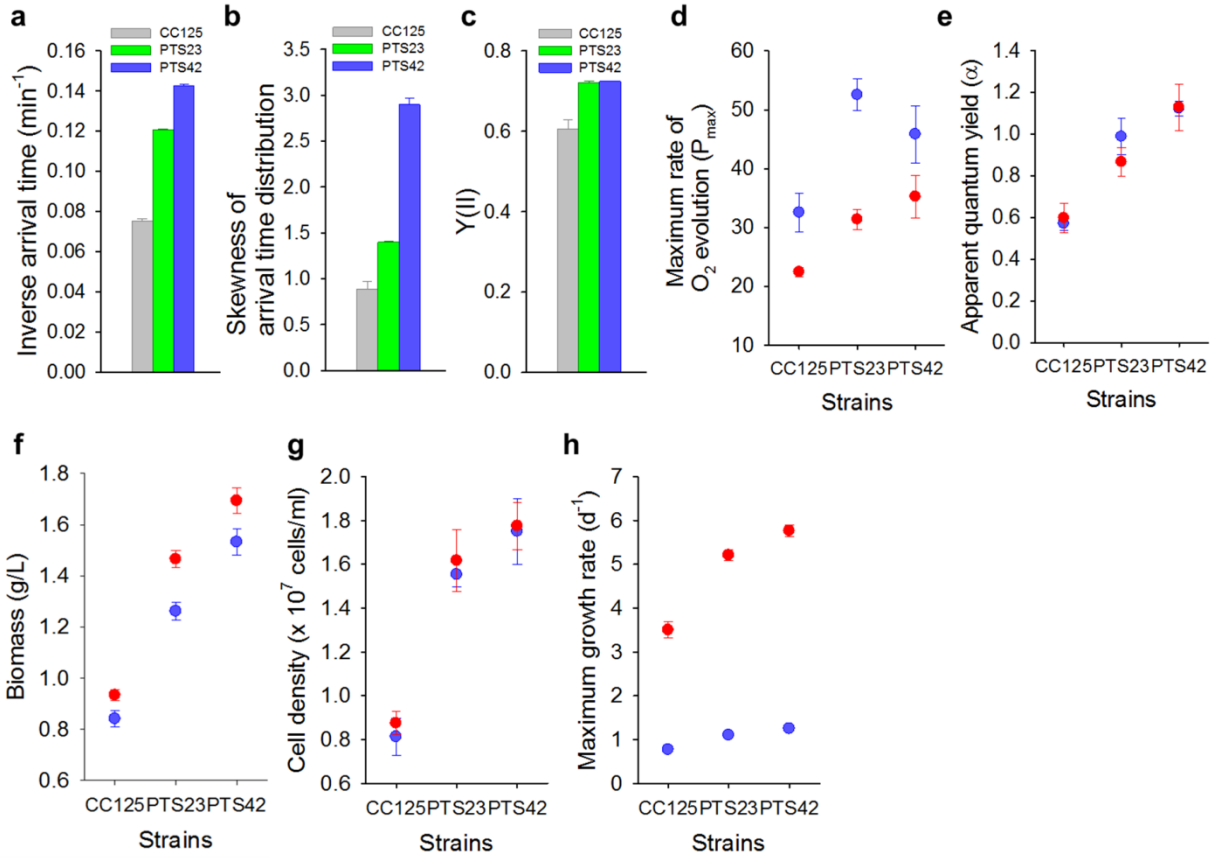

Supplementary Figure S6. Phototactic and photosynthetic characteristics of two mutants (PTS23, PTS42) compared to the wild-type strain. (**a–c**) Inverse average arrival time (**a**), skewness of arrival time distribution (**b**) and PSII operating efficiency (Y(II)) (**c**) of two mutants compared to the wild-type strain. Cells were grown photomixotrophically in TAP medium under continuous low light condition (50 µmol photons m^{-2} s^{-1}). (**d**,**e**) Maximum photosynthetic rates (P_{max}) (**d**) and apparent quantum yield of oxygen evolution (α) (**e**) on a per-cell basis in the two mutants compared to the wild-type strain under continuous low light (50 µmol photons m^{-2} s^{-1}) and high light conditions (300 µmol photons m^{-2} s^{-1}). α, arbitrary unit; P_{max}, nmol O_2 (10^6 cells)$^{-1}$ min^{-1}. (**f–h**) Biomass production (**f**), final cell density (**g**), maximum growth rate (**h**) of the two mutants compared to the wild-type strain in continuous low and high light. Maximum growth rates were calculated from the Gompertz function[40] (**h**). Cells with the same initial cell densities (~5 × 10^5 cells/ml) were grown photoautotrophically in a CO_2 incubator at 5% CO_2. Blue circle: low light, Red circle: high light (**d–h**). All data and error bars are the mean ± SD of three biological replicates.

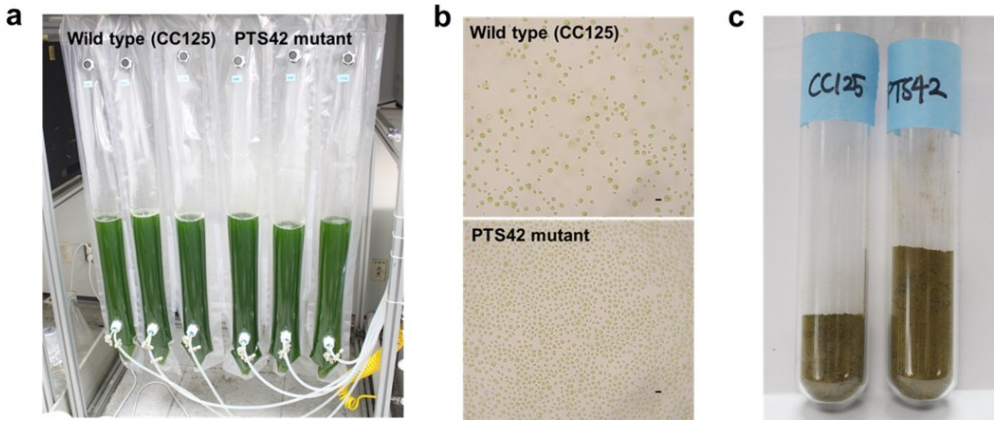

Supplementary Figure S7. Mass culture of the wild-type strain and PTS42 mutant using photobioreactor system. (**a**) Picture showing cultivation of wild type and PTS42 in photobioreactors. (**b**) Representative microscopy images showing different cell densities of wild type and PTS42 mutant at 72 h. Scale bars, 10 μm. (**c**) Picture showing dried cell powder obtained from 2-liter culture broth of wild type and PTS42 mutant. Cells were grown photoautotrophically with the same initial cell densities (~1×10^5 cells/ml) in 3-liter TP medium using a 5-liter photobioreactor at a light intensity of 350 μmol photons m^{-2} s^{-1} by supplying 5% CO_2-enriched air at a flow rate of 50 ml l^{-1} min^{-1}.

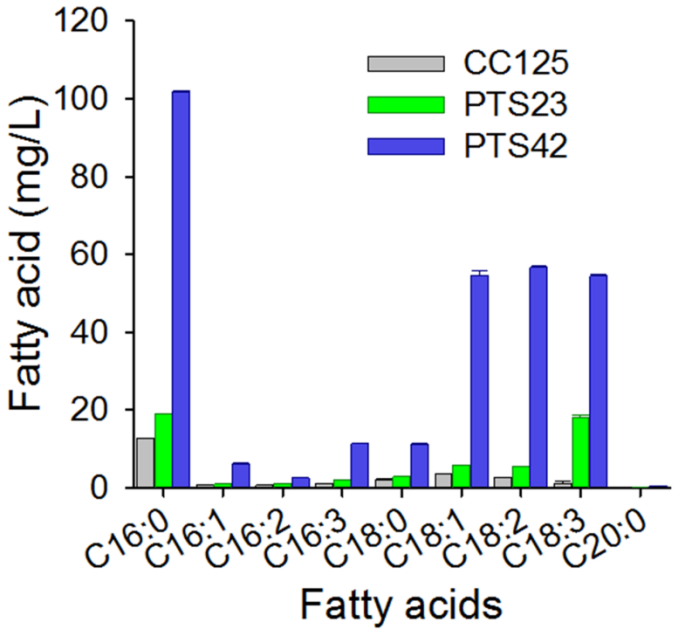

Supplementary Figure S8. Fatty acid production in two mutants (PTS23, PTS42) compared to the wild-type strain. Cells were grown photoautotrophically for 4 days in a CO_2 incubator at 5% CO_2 in TP medium under continuous low light condition (50 µmol photons m^{-2} s^{-1}), and then incubated in TP(-N) media in a CO_2 incubator at 5% CO_2 for 4 days for lipid accumulation. All data and error bars are mean ± SD of three biological replicates.

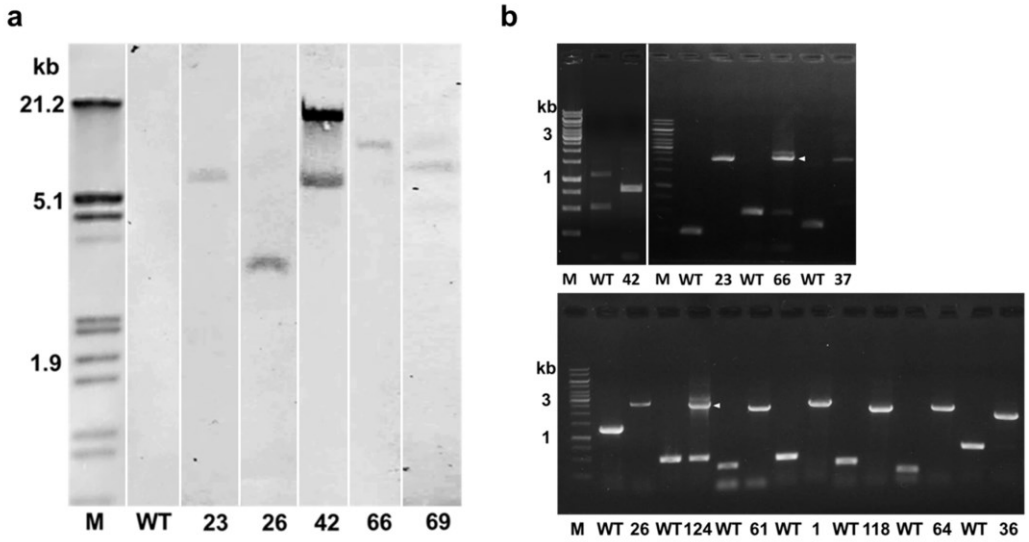

Supplementary Figure S9. Genomic DNA analysis of selected PTS (phototaxis-screening) mutants. (**a**) Southern blot analysis of genomic DNA from five selected PTS mutants (PTS23, 26, 42, 66, 69). Genomic DNA was digested with PstI (PTS23, 42, 66) or PstI & NsiI (PTS26, 69). The 3′ region of the *aph7″* coding sequence was used as a probe. M: Dig-labelled DNA molecular weight marker III (Roche), WT: wild type (CC125). Each number denotes the number of PTS mutants. (**b**) PCR analysis of insertion site in the genomic DNA of PTS mutants. PCR was carried out using specific primers (Supplementary Table S1) targeting flanking sequences on both sides of the marker gene, and amplified product was sequenced. M: GeneRuler 1 kb DNA ladder (Fermentas), WT: wild type (CC125). Each number denotes the number of PTS mutants. 42: PCR product using primers (42R, UP2). The arrow indicates specific amplified product of the mutant. Due to the concatameric insertion of selection marker gene, one additional integration site in PTS42 and one of both flanking sequences in PTS69 were not identified.

Supplementary Table S1. Sequences of oligonucleotides used in this study.

Name	Sequence (5'→3')	Description
UP3	GACTCACCTCCCAGAATTCCTGG	TAIL-PCR (primary), specific primer for upstream sequence[46]
UP2	TCGTTCCGCAGGCTCGCGTAGG	TAIL-PCR (secondary), specific primer for upstream sequence[46]
UP1	TCGAGAAGTAACAGGGATTCTTGTGTCATG	TAIL-PCR (tertiary), specific primer for upstream sequence[46]
DP4	CTTCGAGGTGTTCGAGGAGACCC	TAIL-PCR (primary), specific primer for downstream sequence[46]
DP3	CGCTGGATCTCTCCGGCTTCACC	TAIL-PCR (secondary), specific primer for downstream sequence[46]
DN1	GAACTGGCGCAGTTCCTCTG	TAIL-PCR (tertiary), specific primer for downstream sequence (this study)
RMD227	NTCGWGWTSCNAGC	TAIL-PCR, degenerate primer[36]
iHSU1	ATGACACAAGAATCCCTGTTACTT	Inverse PCR, for upstream sequence
iHSU2	CATAGCGCAAGAAAGAAGCTTG	Inverse PCR, for upstream sequence
iHSD1	CAGTGCTCGCCGAACAGCTTGA	Inverse PCR, for downstream sequence
iHSD2	CGCTGGATCTCTCCGGCTTCACC	Inverse PCR, for downstream sequence (same as DP3)
1F	ACGCATATTTGTCTTGTGCACACA	Sequence specific primer for mutant PTS1
1R	AGGTTCGTAGGTCAGGCAAACAGA	Sequence specific primer for mutant PTS1
23F	AGCCCAGTCACTGTGGAGTCACTTA	Sequence specific primer for mutant PTS23
23R	GCCCTAGGCAGAGTCCAAAGCT	Sequence specific primer for mutant PTS23
26F	TGACTCGATCGCTAAATGCGTTG	Sequence specific primer for mutant PTS26
26R	CCAGCAGAGGTAGGATCCCATTTC	Sequence specific primer for mutant PTS26
36F	AAACCTAGCTATGGTATCATTTCC	Sequence specific primer for mutant PTS36
36R	ACTGGCGTCCCTGCAATGAAAGA	Sequence specific primer for mutant PTS36
37F	GCCCTGCTGTCTTCTGATCTAAGC	Sequence specific primer for mutant PTS37
37R	GCACGAATACTCACGAGTGAATG	Sequence specific primer for mutant PTS37
42R	GGACACCAAGATAGCAAGAAGAAGC	Sequence specific primer for mutant PTS42
61F	TCGAAGAACTGGCAATTCATATGA	Sequence specific primer for mutant PTS61
61R	CTTGAATCGATTTTCTCTTTGTCAG	Sequence specific primer for mutant PTS61
64F	ATGCTTGGTCAGACGGATAACGTA	Sequence specific primer for mutant PTS64
64R	AGTGAGTGACTAGCGGTTGTTTAA	Sequence specific primer for mutant PTS64
66F	GCCAATCATGCCTGCTGTGAGACG	Sequence specific primer for mutant PTS66
66R	AGGCCATTACCTTCACTACAGCG	Sequence specific primer for mutant PTS66
118F	GAGTGAGTATCGCCAAGCAATTGC	Sequence specific primer for mutant PTS118
118R	CTTCTGTCATGTTGAACCTCTC	Sequence specific primer for mutant PTS118
124F	TGTTGGGGTGTAGTTGTAGTTGG	Sequence specific primer for mutant PTS124
124R	CCATGCTGAACTCGTCCATCTGC	Sequence specific primer for mutant PTS124

Supplementary Video S1. Immediate phototactic response of a single cell of *Chlamydomonas reinhardtii* in a microchannel to the changes in the direction of light.

The movie shows the negative phototactic responses of wild type cells (CC125) at the level of single-cell resolution. The direction of light is changed using two green LED lamps at both ends of the microchannel, which are switched on and off alternately.

Supplementary Video S2. Analysis of negative phototactic response using custom software.

The movie shows that cells arrived at observation zone near the outlet chamber are counted, and their arrival times are automatically recorded using custom software.

Supplementary Video S3. Phototactic responses under a 12 h–12 h LD cycle.

The movie shows the phototactic responses of wild type cells (CC125) at different time points (see the text in each panel) under the LD cycle. All video panels were recorded during the same period.

Supplementary Video S4. Comparison of the phototactic responses of two mutants to wild type.

The movie shows the phototactic responses of two mutants with different phototactic responses (left: slow response, right: fast response) and photosynthetic efficiencies (left: low Y(II), right: high Y(II)) compared to the wild type strain (middle, CC125). All video panels were recorded during the same period.